Competitive Pathways via Nonadiabatic Transitions in Photodissociation

DAVID CONROY,† VICTOR ARISTOV,‡ LIN FENG, ANDREI SANOV,|| AND HANNA REISLER*

Department of Chemistry, University of Southern California, Los Angeles, California 90089-0482

Received October 6, 2000

ABSTRACT

Photodissociation processes of molecules and radicals involving multiple pathways and nonadiabatic crossings are studied using the photofragment imaging technique and the core-sampling version of time-of-flight spectroscopy. Capabilities and challenges are illustrated by two systems. The isocyanic acid system demonstrates how interactions among potential energy surfaces can change during dissociation. The hydroxymethyl photodecomposition system highlights Rydberg-valence interactions common in free radicals. The cross-fertilization between theory and experiment is emphasized.

Introduction

The interaction of light with molecules is of both fundamental and practical importance. It affects areas as diverse as ozone depletion, global warming, organic synthesis, polymerization, photosynthesis, and vision. It has fascinated physicists, chemists, and biologists for decades, and its detailed study has resulted in a deeper understanding of the correlation between electronic structure and nuclear motion. In other words, the changes in the electronic environment perceived by the nuclei trigger motions that terminate in decomposition, isomerization, or couplings among potential energy surfaces.

In striving to understand dissociation pathways for polyatomic molecules, the chemical physicist uses as rigorous an application of the fundamental laws of physics as is feasible, in conjunction with chemical intuition based on results of analogous systems (e.g., isovalent, isoelectronic). In the past two decades, great progress has been made in understanding the photoinitiated decomposition of triatomic molecules because of the confluence of theory and experiment. Among the notable successes of the combined experimental/theoretical approach are the detailed state-to-state descriptions of photodissociation on repulsive surfaces[1] and, at the other extreme, unimolecular decomposition from deeply bound surfaces that on average are well-described by statistical theories.[2] In the former case, the correlation between the electronic structure and the forces and torques that act on the departing fragments gives rise to clear experimental fingerprints in product state distributions. In the latter case, the apparently random fluctuations in rates and final state populations give rise, upon averaging, to distributions such as those derived from statistical models.

In our work, we have examined fundamental concepts in the photodissociation of triatomic molecules by choosing systems that are amenable to exact theoretical treatments. As examples of dissociation from a single repulsive surface, we studied the photodissociation of ClNO and FNO, demonstrating mappings of molecular vibrational wave functions into photofragment rotational distributions and quantum mechanical coherent interference control of product-branching ratios.[3,4] We also studied in state-to-state detail the photoinitiated unimolecular decomposition of NO_2 from its *ground* electronic state.[5] By analyzing fluctuations due to overlapping resonances and dynamical signatures in statistical ensembles, we were able to scrutinize the underlying assumptions of the statistical theories.

Despite these notable successes, decompositions from isolated electronic states of triatomic molecules are a minority; usually, different electronic states participate and interact, giving rise to several competitive channels. Quantum mechanical interference can further complicate the picture but, when understood, can be exploited in coherent control of reaction outcomes.[6] The situation with polyatomic free radicals is even more complex because opportunities abound in these open shell systems for couplings among close-lying electronic surfaces, and isomerization is more likely to occur.

With the increase in computational speed, treating five to six atom molecules is now within reach, although many challenges involving ab initio calculations of excited states and bond-breaking processes still exist. Experimentally, the increased complexity of multichannel systems can make detailed state-to-state studies a daunting task.

David Conroy received his Ph.D. in chemistry from USC and is about to start postdoctoral training in JPL, Pasadena.

Vicotr Aristov obtained his Ph.D. in chemistry from USC and is currently a staff member at KLA-Tencor.

Lin Feng is a second year graduate student at USC.

Andrei Sanov received his undergraduate education at the Moscow Institute of Physics and Technology and a Ph.D. from USC in 1996. He was a postdoctoral fellow at JILA, Boulder, with W. C. Lineberger and joined the Chemistry Department of the University of Arizona in 1999. His interests are in mapping orbital dynamics in reactions of negative ions and clusters using photoelectron spectroscopy and imaging.

Hanna Reisler received her undergraduate education at the Hebrew University of Jerusalem, specializing in organic chemistry, and earned a Ph.D. degree in physical chemistry in 1972 from the Weizmann Institute of Science. She was an IAEA postdoctoral fellow at Johns Hopkins University and a group leader in laser development at the Soreq Nuclear Research Center, Israel. She has been at USC since 1977. Her current interests involve dynamics of reactions and photodissociation in the gas phase and at gas−solid interfaces.

* To whom correspondence should be addressed. E-mail: reisler@chem1.usc.edu. Phone: 213-740-7071. Fax: 213-740-3972.

† Present address: NASA/Jet Propulsion Laboratory, 4800 Oak Grove Dr., Pasadena, CA 91109.

‡ Present address: KLA-Tencor Corp., One Technology Drive, Building 5, Milpitas, CA 95035.

|| Present address: Department of Chemistry, The University of Arizona, 1306 E. University Blvd., Tucson, AZ 85721-0041.

10.1021/ar970047y CCC: $20.00
Published on Web 05/23/2001

Therefore, methods capable of giving mechanistic "road maps" more expeditiously are needed, even if they come at the expense of some resolution and state specificity. We are presently exploiting two methods in our quest for understanding complex decompositions: velocity map imaging (i.e., a high-resolution implementation of photofragment ion imaging)[7,8] and the core-sampling variant of time-of-flight (TOF) spectroscopy.[9]

Decomposing systems that are important in realistic environments often involve excitation to bound states that nevertheless couple to dissociative surfaces and give rise to several product channels. A fascinating challenge afforded by these systems is the chemist's dream of exerting control over reaction outcomes (e.g., the branching ratios) by tailoring the excitation conditions. Can we effect "bond-selective" chemistry, that is, obtain chemically distinct channels with good selectivity? We would like ultimately to devise a strategy based on in-depth understanding of the relevant competing processes. If we are less ambitious, we may at least endeavor to find benchmark systems that can be treated by theory, thereby allowing us to confidently predict the outcome.

To illustrate both the present capabilities and the challenges in investigating multichannel photodissociation events, we have chosen two examples from our recent work: isocyanic acid (HNCO) and the hydroxymethyl (CH_2OH) radical. The former illustrates our ability to unravel dissociation pathways in a rather complex system where the interactions among several surfaces change during the dissociation process. It also highlights several fundamental aspects of photoinitiated dynamics and the crucial cross-fertilization between theory and experiment. The hydroxymethyl radical decomposition, which is important in the combustion of methanol, demonstrates the challenges yet to be surmounted, but the success of our initial experiments is a source of optimism for the future. Space limitations prevent us from discussing the excellent work done in other laboratories, but directions for future studies are briefly discussed at the end.

HNCO: Multiple Pathways in Dissociative Coupled States

The photodissociation of HNCO provides an intriguing example of the rich photochemistry that even a simple four-atomic molecule can reveal. Isocyanic acid (HNCO) is implicated in the removal of nitrogen oxides in combustion, in energetic materials combustion, and in interstellar space. It is also a possible intermediate in the reaction H + NCO → NH + CO. Therefore, the mechanisms of its decomposition and chemical reactions are of interest.

The photodissociation of HNCO following excitation to the first excited singlet state, $S_1(^1A'')$, has attracted much attention as it involves a small molecule which nevertheless can dissociate via three channels evolving on three potential energy surfaces (PESs):[10−13]

$$\rightarrow \mathrm{NH}(X^3\Sigma^-) + \mathrm{CO}(X^1\Sigma^+) \qquad D_0(^3\mathrm{NH} + \mathrm{CO}) = 30\,060 \pm 30\ \mathrm{cm}^{-1} \quad (1)$$

$$\mathrm{HNCO} \rightarrow \mathrm{H}(^2\mathrm{S}) + \mathrm{NCO}(X^2\Pi) \qquad D_0(\mathrm{H} + \mathrm{NCO}) = 38\,370 \pm 30\ \mathrm{cm}^{-1} \quad (2)$$

$$\rightarrow \mathrm{NH}(a^1\Delta) + \mathrm{CO}(X^1\Sigma^+) \qquad D_0(^1\mathrm{NH} + \mathrm{CO}) = 42\,750 \pm 30\ \mathrm{cm}^{-1} \quad (3)$$

In what follows, $NH(X^3\Sigma^-)$ is denoted by ^3NH, and $NH(a^1\Delta)$ is denoted by ^1NH.

At ~230 nm, all three channels are open, and issues of state specificity and bond selectivity become important. Indeed, it has been shown that in this wavelength region, the branching ratio among product channels can be changed by a slight variation in the photolysis wavelength.[11] An elegant demonstration of bond-selective chemistry was given by Crim and co-workers.[12,13] They implanted several quanta of excitation in NH stretch vibration of the *ground* electronic state and then photodissociated only the excited molecules. With this double-resonance scheme, they found that channels 1 and 2 increased in population relative to channel 3, compared to results obtained with one-photon excitation. It has become clear, however, that understanding this bond selectivity requires detailed knowledge of the dissociation mechanism, which can be obtained only with the participation of theory.[14−16] Collaboration between theory and experiment has also been crucial to the recent determination (after many years of effort) of the band origin for excitation to $S_1(^1A'')$, which is now placed at 32 450 cm^{-1}, and the assignment of the $S_1 \leftarrow S_0$ vibronic spectrum.[17]

To unravel the dissociation mechanism, several pieces of information are necessary: (i) the potential energy surfaces that participate in the dissociation (the energetically accessible states are S_1, the ground-state S_0, and the first excited triplet state T_1); (ii) the barriers to dissociation on each surface; (iii) the surfaces that couple nonradiatively; (iv) the relevant time scales involved in the competing processes; and (v) the dynamics that govern energy disposal in the products.

Recently, many aspects of HNCO decomposition have become fully understood. For example, it is established that at the wavelength region where state specificity is observed, all three electronic states, S_0, S_1, and T_1, participate. Therefore, nonadiabatic transitions between the S_1 state accessed in the photoexcitation (i.e., the "bright" state) and the other states are of crucial importance in understanding the dissociation dynamics.

In our studies, we use supersonic beams of isolated molecules to achieve a rotational temperature of ~10 K. For detection, we exploit the photofragment imaging technique, and especially its high-resolution velocity map variant,[18] which constitutes a real advance in our quest to elucidate complex dissociation mechanisms. In imaging, products are detected state-selectively (e.g., by laser ionization), and the images afford simultaneous resolution in the mass, frequency, velocity, and angular domains. Often, few images taken at strategic energy regions suffice

to provide mechanistic insights. In this method, pioneered by Houston and Chandler,[7,8] the molecules in the beam are dissociated by laser irradiation. Immediately afterward, a desired product in a specific rovibrational state is tagged by multiphoton ionization and is accelerated with a constant electric field toward a position-sensitive detector. Most of the products acquire recoil velocity in the dissociaton (for example, because of repulsive forces), and the resulting photofragment ion paths deviate from the direction of the electrostatic acceleration. Therefore, most of the ionized products impinge on the detector away from the center, with the impact positions determined by their recoil velocity vectors. The ion impacts lead to fluorescence in a phosphor screen coupled to the detector, and the two-dimensional (2D) distribution of the fluorescence intensities is recorded by a CCD camera. The recorded image can then be transformed back into the original 3D velocity distribution, of which a cut that includes the center is usually displayed. A key element in the experimental arrangement is an immersion ion lens that (i) focuses all ions with the same velocity to the same spot on the detector, even if they originate at different spatial locations, and (ii) provides a "zoom" capability that enables fitting the fastest recoiling products within the detector area.[18] This lens increases the resolution and the dynamic range.

By using energy and momentum conservation, the internal energy distribution of the "dark" product can be inferred since

$$E_{h\nu} - D_0 = E_{\text{int}} + E_{\text{trans}}$$

where $E_{h\nu}$ is the photon energy, D_0 is the dissociation threshold, E_{int} is the internal energy of the fragments, and E_{trans} is the relative translational energy. E_{trans} can be straightforwardly obtained from the velocity distributions.

The angular distribution of the products at each E_{trans} is described by[19]

$$P(E_{\text{trans}},\theta) = [P(E_{\text{trans}})/4\pi]\{1 + \beta[3\cos^2(\theta) - 1]/2\}$$

The effective recoil anisotropy parameter, β, characterizes the angular distribution in terms of the angle θ between the relative directions of the light-polarization vector and the fragment-recoil velocity and ranges between the limiting values of 2 and -1 for parallel and perpendicular transitions. A positive or negative β is associated with a product distribution that peaks, in our arrangement, in either the polar or the equatorial region of the image, respectively. An anisotropic distribution usually corresponds to a characteristic dissociation time scale of ~100−5000 fs (determined relative to the average rotational period of the molecule). The $\beta \sim 0$ value (corresponding to an isotropic angular distribution) is obtained when the dissociation time is much longer than the period of rotation unless other factors cause reduction in anisotropy. Although an exact treatment of β is much more complex, for the purpose of the present discussion, the above simple analysis will suffice.

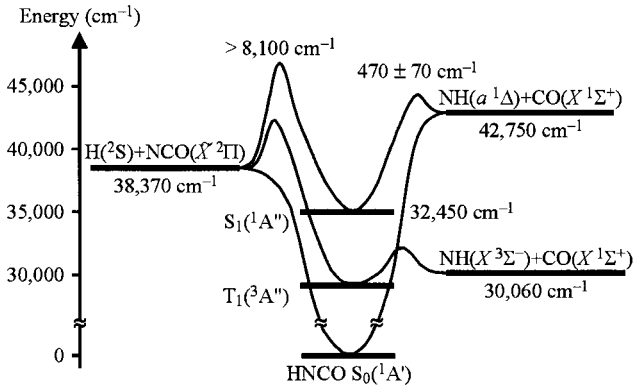

FIGURE 1. Schematic energy level diagram of the three lowest energy dissociation channels of HNCO. See the text for details.

The power of the imaging technique will become clearer when discussing the specific example of HNCO dissociation. In the following, we will often refer to Figure 1, which summarizes what is currently known from experiment and theory about the barriers and energetics of the various surfaces and channels.

Barriers to Dissociation on S_1. Displayed in Figure 2a is a CO image obtained in the 230 nm dissociation of HNCO. The image size was adjusted to include only the contribution from channel 3, and the rotational levels $J_{\text{CO}} \approx 0-2$ of the ground vibrational state of CO ($\nu = 0$) were selected by the probe laser.[20] Notice that this image exhibits clear anisotropy, which immediately indicates that the dissociation lifetime is shorter than the period of rotation (<1 ps). The image was transformed into the corresponding 3D recoil distribution by means of the Abel inversion;[21] a 2D cut through the reconstructed 3D distribution is shown in Figure 2b. Visual inspection reveals that the translational energy release for CO($\nu = 0$, $J \approx 0-2$) is concentrated near the maximum value allowed by energy conservation. Thus, ^{1}NH produced in correlation with low rotational levels of CO is rotationally cold.[22]

More quantitative information on the ^{1}NH correlated distribution is gained from the CO recoil velocity distribution (solid line in Figure 2c) obtained by integrating the 3D distribution along the angular coordinates. The dashed traces show schematically the positions of the correlated ^{1}NH rotational levels as calculated from energy conservation. Obviously, the lowest rotational levels of CO correlate mostly with $J_{\text{NH}} = 2$, which is the lowest possible rotational level for ^{1}NH. Although J_{NH} levels up to 6 are energetically allowed, $J_{\text{NH}} = 3$ is the highest observed level. The small signal at the highest velocities is due to fast recoiling CO from channel 1.[11]

A qualitatively different situation is depicted in Figure 2d−f.[11] Here, the monitored rotational level is predominantly $J_{\text{CO}} = 14$, which is at the tail of the observed CO rotational distribution. Two differences are immediately discernible: (i) higher rotational levels of ^{1}NH are populated—up to the energetically allowed maximum—and (ii) these higher levels exhibit less anisotropy than in Figure 2a. These results, as well as those obtained for other J_{CO} levels, reveal that at ~230 nm, two pathways contribute to the formation of channel 3. Most of the CO rotational

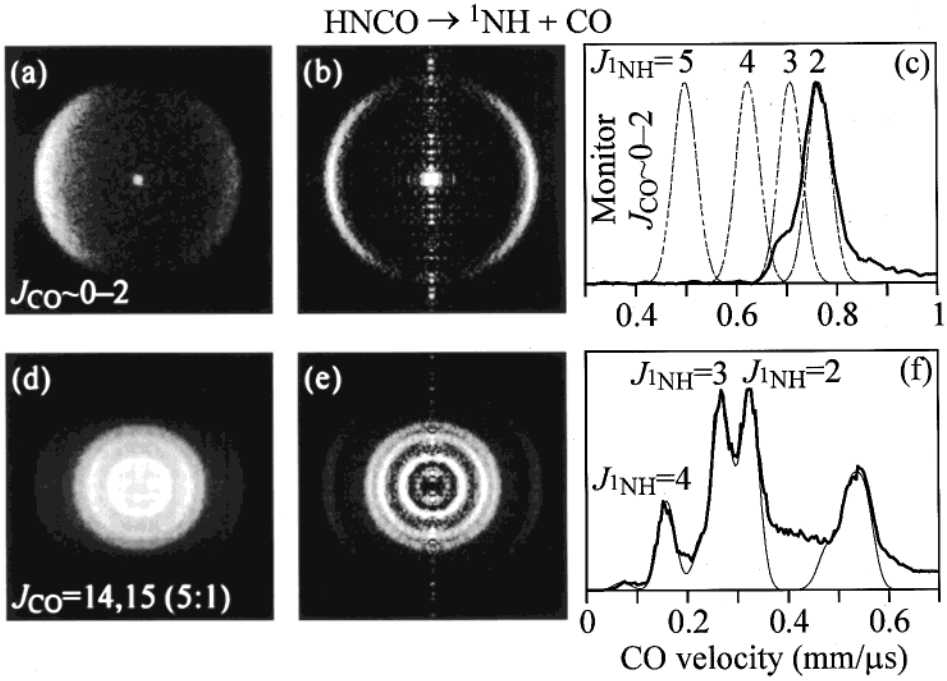

FIGURE 2. CO images obtained at ~230.1 nm in a one-color experiment monitoring (a) $J_{CO} = 0-2$ and (d) $J_{CO} = 14, 15$. Panels (b) and (e) represent 2D cuts through the 3D velocity distributions of images (a) and (d), respectively. In panels (c) and (f) the corresponding velocity distributions derived from the reconstructed 3D images are shown in thick lines. The thin dashed lines in (c) show positions of ^{1}NH levels. The thin solid lines in (f) show fits to the velocity distributions. The feature at ~0.5 mm/μs in (f) is from dissociation of a hot band.

levels are generated by fast dissociation on S_1 over a small barrier (see below), while the highest CO levels associated with channel 3 are correlated with higher ^{1}NH rotational levels and are produced by a much slower dissociation process. As we shall see later, the slower process evolves on the deeply bound S_0 ground surface. We fit the velocity distributions in both cases by using $D_0(^1\text{NH} + \text{CO}) = 42\,750 \pm 30$ cm^{-1}, which gives the most accurate value to date for the thermochemical value of this channel.[11] From images at progressively lower photolysis energies, we estimated the barrier to direct dissociation on S_1 as 470 $\pm$ 60 cm^{-1}.[11] It is gratifying that two high-level ab initio calculations give values similar to our experimental measurement.[16,23]

Referring to Figure 1, we see that channel 2 correlates with dissociation on S_1, S_0, and T_1. NCO products are detected at their thermochemical threshold, as seen in Figure 3. This figure also demonstrates that when the photolysis wavelength is scanned while monitoring the NCO and ^{3}NH products, the photofragment yield spectra exhibit narrow features. The reason is that the S_1 state is bound in this region, and NCO production must evolve via nonadiabatic couplings to a lower electronic state. If the dissociative state is the deeply bound S_0 state, then we expect dissociation to occur on a time scale much longer than a rotational period of the parent. This should lead to a product angular distribution that is isotropic, *even when the products from the direct dissociation on S_1 (channel 3) are anisotropic*. Figure 4 compares the images of $J_{CO} \approx 0-2$ and H atom images obtained at ~230 nm via channels 3 and 2, respectively.[11] Clearly, the H atom image is isotropic, typical of a relatively slow unimolecular

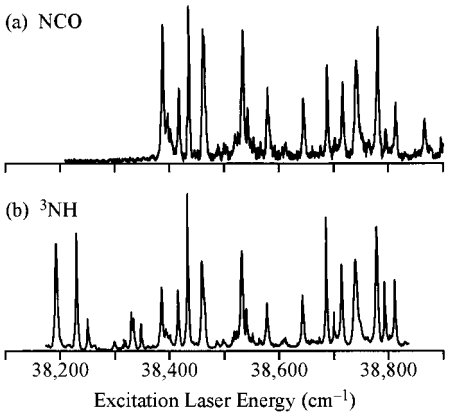

FIGURE 3. Photofragment yield spectra of HNCO obtained in the region near the threshold of channel 2 obtained by monitoring (a) NCO and (b) ^{3}NH, while scanning the photolysis laser.

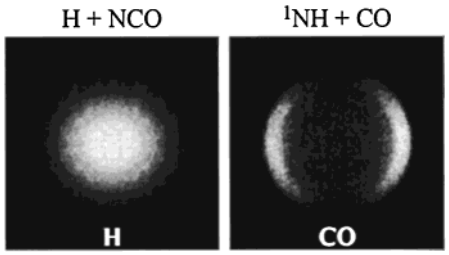

FIGURE 4. Comparison of H and CO ($J = 0-2$) photofragment ion images obtained at ~230 nm. Notice the difference in anisotropy.

decomposition, and has a broad velocity distribution (corresponding to a broad NCO rovibrational distribution). The NCO energy distribution is indeed well-described by a statistical model applied to dissociation on S_0.[24] Because

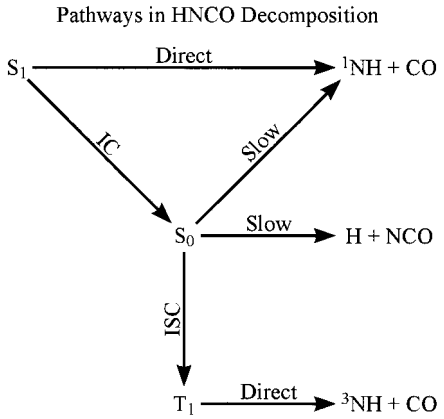

FIGURE 5. Pathways important in the photodissociation of HNCO at 280−215 nm, including internal conversion (IC) and intersystem crossing (ISC).

we have already shown that at 230 nm fast dissociation on S_1 leads to channel 3, the S_1 barrier to channel 2 must be much higher. How high is it? Our H atom images remain isotropic up to ~8100 cm^{-1} above the H + NCO threshold, and theory predicts barriers in the range 8000−11 000 cm^{-1}.[16,23] The respective heights of the barriers to channels 2 and 3 are indicated in Figure 1.

Dissociation Mechanism and Nonadiabatic Couplings. It is evident that channels 1 and 2 must evolve via nonadiabatic couplings to lower-lying surfaces. The lack of anisotropy in the images of channel 2 suggests that it evolves on a time scale of at least 5−10 ps; therefore, the dissociation takes place on the deeply bound S_0 state (rather than on T_1). What is the mechanism of formation of channel 1?

Channel 1 dissociation plays a role at all photolysis energies relevant to this study. [10] It must involve intersystem crossing to T_1—the only state correlating with ^{3}NH + CO products (Figure 1). Mebel et al. calculated an exit barrier of 1500 cm^{-1} on the T_1 potential energy surface;[14] hence, dissociation on T_1 at the experimental photolysis energies should be prompt. By "zooming" the imaging system to also capture the fast CO fragments that are generated via channel 1, we obtain an estimate of the time scale for the appearance of this channel.[11] Surprisingly, the images obtained for *fast* CO have *isotropic velocity distributions*; that is, a relatively long-lived intermediate state must be involved in the dissociation. A picture that explains these observations and also agrees with the theory involves the dissociation route $S_1 \rightarrow S_0 \rightarrow T_1 \rightarrow {}^3$NH + CO, where the slowest step is the intersystem crossing.[16]

The main pathways at 280−215 nm are shown schematically in Figure 5. It is intriguing that high above the S_1 barrier to channel 3 dissociation, all three products are observed, even though surface crossings must compete with direct dissociation. What is the explanation for such behavior?

The answer comes from ab initio theoretical calculations.[14−16] The branching ratios among the channels are determined by the locations of crossing seams for nonadiabatic transitions between surfaces, the strengths of the coupling matrix elements, and the regions accessed on the S_1 potential energy surface by the *dissociating* molecule. Stretching the N−C bond, along with bending motions, promotes S_1−S_0 internal conversion; that is, the same motions that are involved in S_1 dissociation to channel 3 are also those that promote nonadiabatic transitions. Thus, S_1 becomes more "leaky" at large N−C separations, and channel 2 is not entirely quenched even when channel 3 is open. Calculations also reveal that the S_1−T_1 crossing seam is located at energies higher than the threshold to channel 3, explaining why accessing T_1 directly from S_1 is unlikely and crossing to S_0 first is favored. Once on S_0, there is competition between unimolecular reaction to channel 2 and intersystem crossing to T_1 (leading to channel 1). The relative rates of these processes depend strongly on excitation wavelength and have been determined experimentally from branching ratios of the two channels.[24]

Despite the great progress in the mechanistic understanding of the one-photon dissociation of HNCO, the fluctuations in the branching ratios in the wavelength region where all three channels are open (<230 nm) are still poorly understood.[11] In addition, the question remains open as to why exciting NH stretch vibrations so strongly affects the branching ratios between channel 3 and 1 + 2. Does dissociation on S_1 become slower or is the internal conversion to S_0 faster? Recent calculations tend to favor the former.[15] The important point is that benchmark data now exist that can test the calculations and explain the influence of nuclear motions in regions of the potential energy surface far from equilibrium. In addition, Crim and co-workers, who have used double-resonance excitation and dissociation, have learned much about the energy flow in the vibrationally excited ground-state molecule.[25,26]

Decomposition of CH_2OH: Rydberg and Valence-State Interaction

Our second example involves a molecular system of even greater complexity. The $CH_3O \leftrightarrow CH_2OH$ system serves as an excellent prototype for examining decomposition pathways of oxygen-containing free radicals relevant to combustion. It is important in methanol combustion, where reactions of CH_2OH are very fast.[27] It also provides rich opportunities for influencing decomposition pathways via multiple resonance excitation schemes favoring isomerization, direct dissociation, or predissociation via surface crossings.[28,29] The spectroscopy and photophysics/photochemistry of these isomers justly attracted much attention, and good compilations of references can be found in refs 28 and 30 for CH_3O and in ref 31 for CH_2-OH. The accrued experimental and theoretical knowledge highlights the complexity of this system and the need for additional studies.

One of the main differences between radicals and molecular species is the low ionization energy of radicals. This is expected, since removal of an unpaired electron in the radical often leads to a closed shell, stable ionic species. Below the ground state of the ion lie Rydberg states of the neutral radical; that is, states with the

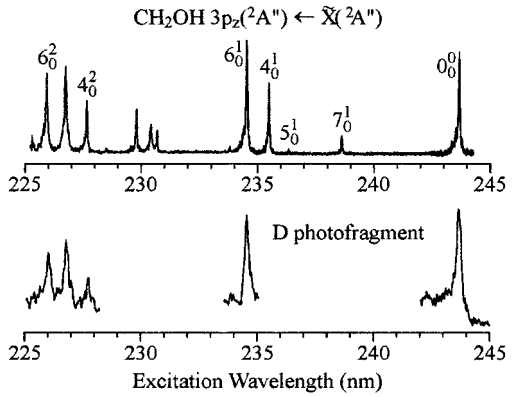

FIGURE 6. (Upper panel) Absorption spectrum of CH_2OD. (Lower panel) D atom photofragment R signal obtained under the same excitation conditions.

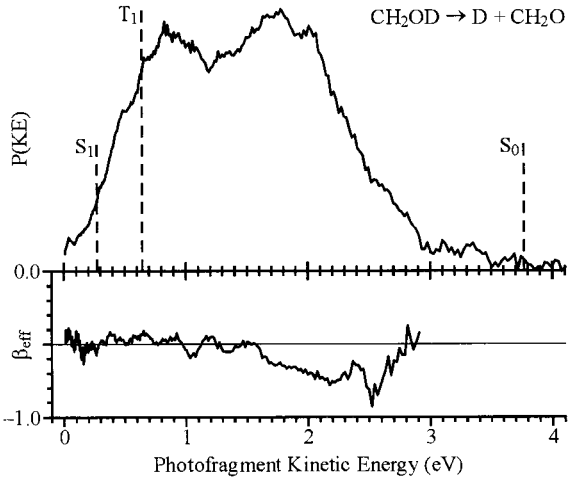

FIGURE 7. (Upper panel) Total translational energy distribution of the recoiling fragments. The maximum translational energies allowed for channels involving CH_2O in the ground, S_1, and T_1 states are shown in dashed lines. (Lower panel) β_{eff} as a function of translational energy, as a measure of the angular distribution of the fragments.

unpaired electron promoted to a high-*n* quantum number and whose nuclear geometries are similar to that of the ion. These states, which correlate with excited electronic states of the products, are usually bound. There are two properties characterizing the Rydberg states that affect their dissociation dynamics:[32] (i) they lie at energies lower than or similar to the (often repulsive) excited valence states and (ii) their electronic wave functions, which are atomic-like and lie far from the nuclei, do not overlap well with the valence-state wave functions, which are closer to the nuclei but may extend over several atoms. This makes nonadiabatic couplings between the excited Rydberg state and the lower valence states inefficient and results in absorption spectra with distinct vibronic structures.

Unraveling the mechanisms of radical decomposition offers challenges and complexities far exceeding those of stable molecules; therefore, only a few systems have been treated in detail. As an illustration, we present here first results on the decomposition of the hydroxymethyl radical from the $3p_z$ Rydberg state; its band origin lies at ~244 nm and its ionization potential is ~7.56 eV.[33] Following $3p_z$ excitation, the radical can decompose to several chemically distinct channels: (1) $H + CH_2O(S_0, T_1, S_1)$; (2) $H + CHOH$; (3) $H_2 + HCO$; (4) $H + H_2 + CO$; and (5) $OH + CH_2$. In addition, the isomerization $CH_2OH \leftrightarrow CH_3O$ may precede dissociation.[29,34]

Compounding the challenges are difficulties in cleanly preparing intense beams of reactive radicals. In our work, beams of CH_2OH radicals are prepared by the reaction between Cl atoms and methanol in the throat of a supersonic nozzle.[35] Fortunately, a good diagnostic exists for hydroxymethyl,[31] and the upper panel of Figure 6 shows the $3p_z(A'') \leftarrow X(A'')$ absorption spectrum obtained with CH_2OD in a molecular beam. The spectrum exhibits a clear vibronic structure but no rotational structure, placing the lifetime of the excited state at <1 ps.[35] More importantly, the same spectrum is obtained when scanning the wavelength of the photolysis laser while monitoring the D product by REMPI with a second laser. This proves that the D fragment is a product of the dissociation of CH_2OD.[34]

Additional mechanistic insight is obtained by looking at the kinetic energy (KE) and angular distributions of D atoms obtained following excitation to the origin band of the $3p_z(A'')$ state (Figure 7).[34] In the core-sampling variant of the TOF technique, a small (~4 mm diameter) aperture is placed in front of the ion detector, limiting detection to only those photofragments that are ejected in a direction parallel or antiparallel to the TOF axis.[9] Thus, a speed distribution is directly obtained from which the KE distribution can be easily derived.

In Figure 7 we also mark the highest KE that is associated with a CH_2O photofragment in its ground S_0 state or in the excited T_1 and S_1 states. Clearly, most of the CH_2O is produced in the ground state, but a small fraction, at low KE, may be excited to S_1 and/or T_1 and is associated with much slower D products. The angular distribution depicted in the lower panel of Figure 7 indicates that dissociation is fast and likely proceeds via predissociation with direct O−D fission. Also intriguing is the preliminary finding that when the $3p_z$ state is excited to higher vibrational levels, strong D peaks appear with low KEs, suggesting that perhaps the fraction of electronically excited formaldehyde increases.[36]

Experiments involving CH_2OH and its isotopomers are still ongoing and continue to reveal intriguing, and occasionally surprising, results. For example, we find H products from CH_2OD with KE much lower than D, possibly deriving from C−H bond scission.[36] Likewise it appears that different isotopomers (CH_2OH, CD_2OH, and CH_2OD) give rise to different branching ratios in the dissociation. With the tools now at hand, experimental data will be generated soon with high degrees of specificity and resolution, and it is hoped that theory will aid in the future in unraveling the nonadiabatic transitions and state couplings responsible for CH_2OH dissociation.

Opportunities and Challenges

One of the greatest challenges in studying polyatomic photodissociation is the multitude of possible outcomes that can result from subtle interactions that couple surfaces. When the coupling matrix elements are weak our intuition often fails, and results from one wavelength regime cannot be carried over to another. In contrast to dissociation from deeply bound surfaces that can be well described by statistical theories, understanding photodissociation from weakly bound or repulsive surfaces demands a molecule-specific joint experimental and theoretical effort. The rapid developments in experiment and theory promise to yield new insights and opportunities; in particular, extensions to ground-state dynamics of radicals are now within reach.

The knowledge gained from such studies will help in understanding photochemical processes characteristic of those encountered in the environment, including the upper atmosphere and stratosphere. Currently, there is increased recognition that discrepancies between atmospheric modeling and observations result from processes that may involve weak nonadiabatic interactions, long wavelength tails of absorption curves, etc. Likewise, the importance of radicals and vibrationally excited or electronic metastable photofragments has been under-appreciated. In fact, only recently it has been concluded in a joint paper on the photochemistry of ozone by several senior investigators that, "A key point is that the dissociation of internally excited species and spin-forbidden processes, exotic as they may sound, are occurring in something as globally and socially important as the atmosphere." [37] It is also clear that the fate of polyatomic radicals created in the primary photolysis step needs to be elucidated. These radicals may be generated with high internal and/or translational energy, but their subsequent reactive pathways are poorly understood. Investigations of radical decompositions are in their infancy and, because of experimental challenges, are not likely to produce quick answers. Moreover, much of what has been discovered has been unanticipated and is still awaiting a parallel theoretical effort. For example, recent results from our laboratory show that although the methyl radical absorbs only in the far UV, the chloromethyl radical has strong absorptions at 230−300 nm, leading to production of Cl atoms. In this wavelength region, the solar flux is high, and these processes, therefore, need to be taken into account in modeling.

This work was supported by the Department of Energy and the National Science Foundation. It is based on results obtained by previous and present co-workers, whose hard work (cited in the reference section) made these studies possible. We also benefited greatly from discussions with D. W. Chandler, F. F. Crim, C. Wittig, R. Schinke, K. Morokuma, and J. Hudgens.

References

(1) Schinke, R. *Photodissociation Dynamics*; University Press: Cambridge, 1993.
(2) Baer, T.; Hase, W. L. *Unimolecular Reaction Dynamics: Theory and Experiments;* University Press: Oxford, 1996.
(3) Qian, C. X. W.; Ogai, A.; Brandon, J.; Ban, Y. Y.; Reisler, H. Photodissociation Dynamics and the Spectroscopy of Fast-Evolving States. *J. Phys. Chem.* **1991**, *95*, 6763−6774.
(4) Ogai, A.; Brandon, J.; Reisler, H.; Suter, H. U.; Huber, J. R.; Dirke, M. V.; Schinke R. Mapping of Parent Transition State Wave Functions into Product Rotations: An Experimental and Theoretical Investigation of the Photodissociation of FNO. *J. Chem. Phys.* **1991**, *96*, 6643−6653.
(5) Reid, S. A.; Reisler, H. The Unimolecular Reaction of NO_2: Overlapping Resonances, Fluctuations and the Transition State. *J. Phys. Chem.* **1996**, *100*, 474−487.
(6) Reid, S. A.; Brandon, J. T.; Reisler, H. Controlling Dissociation Pathways via Fano Profiles: NO State Distributions in FNO(S_1) Decomposition. *J. Phys. Chem.* **1993**, *97*, 5540−543.
(7) Houston, P. L. Snapshots of Chemistry: Product Imaging of Molecular Reactions. *Acc. Chem. Res.* **1995**, *28*, 453−460.
(8) Heck, A. J. R.; Chandler, D. W. Imaging Techniques for the Study of Chemical Reaction Dynamics. *Annu. Rev. Phys. Chem.* **1995**, *46*, 335−372.
(9) Syage, J. A. Photofragment Imaging by Sections for Measuring State-Resolved Angle-Velocity Differential Cross Sections. *J. Chem. Phys.* **1996**, *105*, 1007−1022.
(10) Droz-Georget, T.; Zyrianov, M.; Sanov, A.; Reisler, H. Photodissociation of HNCO: Three Competing Pathways. *Ber. Bunsen-Ges. Phys. Chem.* **1997**, *101*, 469−477.
(11) Zyrianov, M.; Droz-Georget, T.; Reisler, H. Recoil Anisotropies in the Photoinitiated Decomposition of HNCO. *J. Chem. Phys.* **1999**, *110*, 2059−2068.
(12) Brown, S. S.; Berghout, H. L.; Crim, F. F. Vibrational State Controlled Bond Cleavage in the Photodissociation of Isocyanic Acid (HNCO). *J. Chem. Phys.* **1995**, *102*, 8440−8447.
(13) Berghout, H. L.; Brown, S. S.; Delgado, R.; Crim, F. F. Nonadiabatic Effects in the Photodissociation of Vibrationally Excited HNCO: The Branching Between Singlet ($a^1\Delta$) and Triplet ($X^3\Sigma^-$) NH. *J. Chem. Phys.* **1998**, *109*, 2257−2263.
(14) Mebel, A. M.; Luna, A.; Lin, M. C.; Morokuma, K. A Density Functional Study of the Global Potential Energy Surfaces of the [H,C,N,O] System in Singlet and Triplet States. *J. Chem. Phys.* **1996**, *105*, 6439−6454.
(15) Klossika, J. J.; Schinke, R. The Photodissociation of HNCO in the S_1 Band: A Five-Dimensional Classical Trajectory Study. *J. Chem. Phys.* **1999**, *111*, 5882−5896.
(16) Stevens, J. E.; Cui, Q.; Morokuma, K. An *Ab Initio* Study of the Dissociation of HNCO in the S_1, Electronic State. *J. Chem. Phys.* **1998**, *108*, 1452−1458.
(17) Berghout, H. L.; Crim, F. F.; Zyrianov, M.; Reisler, H. The Electronic Origin and Vibrational Levels of the First Excited Singlet State of Isocyanic Acid (HNCO). *J. Chem. Phys.* **2000**, *112*, 6678−6688.
(18) Parker, H. H.; Eppink, A. Velocity Map Imaging of Ions and Electrons Using Electrostatic Lenses: Applications in Photoelectron and Photofragment Ion Imaging of Molecular Oxygen. *Rev. Sci. Instrum.* **1997**, *68*, 3477−3484.
(19) Gordon, R. J.; Hall, G. E. Application of Doppler Spectroscopy to Photofragmentation. *Adv. Chem. Phys.* **1996**, *XCVI*, 1−50.
(20) Droz-Georget, T.; Zyrianov, M.; Reisler, H.; Chandler, D. W. Correlated Distributions in the Photodissociation of HNCO to NH($X^3\Sigma^-$, $a^1\Delta$) + CO($X^1\Sigma^+$) Near the Barrier to S_1. *Chem. Phys. Lett.* **1997**, *276,* 316−324.
(21) Bracewell, R. N. In *The Fourier Transform and its Applications*; McGraw-Hill: New York, 1986.
(22) Sanov, A.; Zyrianov, M.; Droz-Georget, T.; Reisler, H. Photofragment Imaging of HNCO Decomposition: Angular Anisotropy and Correlated Distributions. *J. Chem. Phys.* **1997**, *106*, 7013−7022.
(23) Klossika, J.-J.; Flöthmann, H.; Beck, C.; Schinke, R.; Yamashita, Y. The Topography of the HNCO(S_1) Potential Energy Surface and Its Implications for Photodissociation Dynamics. *Chem. Phys. Lett.* **1997**, *276*, 325−333.
(24) Zyrianov, M.; Sanov, A.; Droz-Georget, T.; Reisler, H. Photoinitiated Decomposition of HNCO near the H+NCO Threshold: Centrifugal Barriers and Channel Competition. *J. Chem. Phys.* **1999**, *110*, 10774−10783.
(25) Coffey, M. J.; Berghout, H. L.; Woods, E., III; Crim, F. F. Vibrational Spectroscopy and Intramolecular Energy Transfer in Isocyanic Acid (HNCO). *J. Chem. Phys.* **1999**, *110*, 10850−10863.
(26) Brown, S. S.; Berghout, H. L.; Crim, F. F. Raman Spectroscopy of the N−C−O Symmetric (ν_3) and Antisymmetric (ν_2) Stretch Fundamentals in HNCO. *J. Chem. Phys.* **1997**, *107*, 9764−9772.
(27) Pagsberg, P.; Munk, J.; Sillesen, A.; Anastasi, C. UV Spectrum and Kinetics of Hydroxymethyl Radicals. *Chem. Phys. Lett.* **1988**, *146*, 375−381.
(28) Osborn, D. L.; Leahy, D. J.; Neumark, D. M. Photodissociation Spectroscopy and Dynamics of CH_3O and CD_3O. *J. Phys. Chem.* **1997**, *101*, 6583−6592.

(29) Walch, S. P. Computed Barrier Heights for H + CH_2O ↔ CH_3O ↔ CH_2OH. *J. Chem. Phys.* **1993**, *98*, 3076−3077.
(30) Powers, D. E.; Pushkarsky, M.; Miller, T. A. Rovibronic Analysis of the Laser-Induced Fluorescence Excitation Spectrum of the Jet-Cooled Methoxy Radical. *J. Chem. Phys.* **1997**, *106*, 6863−6877.
(31) Johnson, R. D.; Hudgens, J. W. Structural and Thermodynamical Properties of Hydroxymethyl (CH_2OH) Radicals and Cations Derived from Observations of B $^2A'$ (3p) ← X $^2A'$ Electronic Spectra and from ab Initio Calculations. *J. Phys. Chem.* **1996**, *100*, 19874−19890.
(32) Sandofry, C. The Ultraviolet Absorption Spectra of Organic Molecules: Valence-Shell and Rydberg Transitions. *Top. Curr. Chem.* **1979**, *86*, 91−138.
(33) Dyke, J. M.; Ellis, A. R.; Jonathan, N.; Keddar, N.; Morris, A. Observation of the CH_2OH Radical in the Gas Phase by Vacuum Ultraviolet Photoelectron Spectroscopy. *Chem. Phys. Lett.* **1984**, *111*, 207−210.
(34) Aristov, V.; Conroy, D.; Reisler, H. Symmetry and Lifetime of the Hydroxymethyl Radical in the $3p_Z$ Rydberg State. *Chem. Phys. Lett.* **2000**, *318*, 393−401.
(35) Conroy, D.; Aristov, V.; Feng, L.; Reisler, H. Predissociation of the Hydroxymethyl Radical in the $3p_Z$ Rydberg State: Formaldehyde + Hydrogen Atom Channel. *J. Phys. Chem.* **2000**, *104*, 10288.
(36) Feng, L.; Khodykin, O.; Reisler, H. Unpublished results, 2000.
(37) Ravishankara, A. R.; Hancock, G.; Kawasaki, M.; Matsumi, Y. Photochemistry of Ozone: Surprises and Recent Lessons. *Science* **1998**, *280*, 60−61.

AR970047Y